Nanotube Superfiber Materials
Changing Engineering Design

Edited by

Mark J. Schulz

Vesselin N. Shanov

Zhangzhang Yin

Notice
No responsibility is assumed by the publisher for any injury and/or damage to persons
or property as a matter of products liability, negligence or otherwise, or from any use or
operation of any methods, products, instructions or ideas contained in the material herein.
Because of rapid advances in the medical sciences, in particular, independent verification
of diagnoses and drug dosages should be made

For information on all William Andrew publications
visit our web site at store.elsevier.com

Printed and bound in the US

13 14 15 16 17   10 9 8 7 6 5 4 3 2 1

Working together
to grow libraries in
developing countries

www.elsevier.com • www.bookaid.org

A Review on the Design of Superstrong Carbon Nanotube or Graphene Fibers and Composites

18

Nicola Pugno

Laboratory of Bio-Inspired and Graphene Nanomechanisms, Center for Materials and Microsystems, Fondation Bruno Kessler, Povo, Italy

CHAPTER OUTLINE

18.1 INTRODUCTION

A space elevator basically consists of a cable attached to the Earth surface for carrying payloads into space [1]. If the cable is long enough, i.e. around 150 Mm (a value that can be reduced by a counterweight), the centrifugal forces exceed the gravity of the cable that will work under tension [2]. The elevator would stay fixed geosynchronously; once sent far enough, climbers would be accelerated by the Earth's rotational energy. A space elevator would revolutionize the methodology for carrying payloads into space at low cost, but its design is very challenging. The most critical component in the space elevator design is undoubtedly the cable [3−5] that requires a material with very high strength and low density.

Considering a cable with constant cross section and a vanishing tension at the planet surface, the maximum stress−density ratio, reached at the geosynchronous orbit, is for the Earth equal to 63 GPa/(1300 kg/m^3), corresponding to 63 GPa if

the low carbon density is assumed for the cable. Only recently, after the rediscovery of carbon nanotubes [6], such a large failure stress has been experimentally measured, during tensile tests of ropes composed of single-walled carbon nanotubes (SWCNTs) [7] and multiwalled carbon nanotubes consist of graphene [8], both expected to have an ideal strength of ∼100 GPa. Note that for steel (density of 7900 kg/m^3 and maximum strength of 1.5 GPa), the maximum stress expected in the cable would be of 383 GPa, whereas for Kevlar (density of 1440 kg/m^3 and strength of 3.6 GPa) of 70 GPa, both much higher than their strengths [3].

However, an optimized cable design must consider a uniform tensile stress profile rather than a constant cross-sectional area [2]. Accordingly, the cable could be built of any material by simply using a large enough taper ratio, that is the ratio between the maximum (at the geosynchronous orbit) and minimum (at the Earth's surface) cross-sectional area. For example, for steel or Kevlar, a giant and unrealistic taper ratio would be required, 10^{33} or 10^8, respectively, whereas for carbon nanotubes and graphene, it must theoretically be only 2^9. Thus, the feasibility of the space elevator seems to become only currently plausible [9,10] thanks to the discovery of carbon nanotubes. The cable would represent the largest engineering structure, hierarchically designed from the nano- (single nanotube or graphene ribbon with length of the order of 100 nm) to the megascale (space elevator cable with a length of the order of 100 Mm). Pushed by this problem we have worked on the design of nanotube or graphene fibers and composites during the last ten years.

In this chapter, the asymptotic analysis on the role of defects for the nanotubes or graphene fibers and composites, based on new theoretical deterministic and statistical approaches of quantized fracture mechanics (QFM) proposed by the author [11−14], and their extension to nonasymptotic regimes, elastic-plasticity, rough cracks and finite domains are reviewed. The role of thermodynamically unavoidable atomistic defects with different size and shape is thus quantified on brittle fracture, fatigue and elasticity for nanotubes, graphene and related bundles and composites. The results are compared with atomistic and continuum simulations and nanotensile tests Specific key simple formulas for the design of a flaw-tolerant space elevator megacable are reported, suggesting that it would need a taper ratio (for uniform stress) of about 1-2 orders of magnitude larger than as today erroneously proposed.

The chapter is organized in 10 short sections, as follows. After this introduction, reported as the first section, we start calculating the strength of nanotube and graphene bundles and composites by using ad hoc hierarchical simulations, discussing the related size effect. In Section 3, the strength reduction of a single nanotube or graphene ribbon and of a nanotube bundle containing defects with given size and shape is calculated; the taper ratio for a flaw-tolerant space elevator cable is accordingly derived. In Section 4, elastic-plastic (or hyperelastic) materials, rough cracks and finite domains are discussed. In Section 5, the fatigue life time is evaluated for a single nanotube or graphene and for a related bundle. In Section 6, the related Young's modulus degradations are quantified. In Sections 7 and 8, we compare our results on strength and elasticity with atomistic simulations and tensile tests of carbon nanotubes. In Section 9, we demonstrate that

defects are thermodynamically unavoidable, evaluating the minimum defect size and corresponding maximum achievable strength. In Section 10, the fiber or composite design against sliding failure is presented. The last section presents our concluding remarks.

18.2 HIERARCHICAL SIMULATIONS AND SIZE EFFECTS

To evaluate the strength of carbon nanotube cables, the hierarchical fiber bundle model, formerly proposed [3], has been adopted [15]. Multiscale simulations are necessary in order to tackle the size scales involved, spanning over ~ 10 orders of magnitude from nanotube/graphene length (~ 100 nm) to kilometer-long cables, and also to provide useful information about cable scaling properties with length.

The cable is modeled as an ensemble of stochastic "springs", arranged in parallel sections. Linearly increasing strains are applied to the fiber bundle, and at each algorithm iteration, the number of fractured springs is computed (fracture occurs when local stress exceeds the nanotube graphene failure strength) and the strain is uniformly redistributed among the remaining intact springs in each section.

In silico stress—strain experiments have been carried out according to the following hierarchical architecture. Level 1: the nanotubes graphene (single springs, Level 0) are considered with a given elastic modulus and failure strength distribution and composed a 40×1000 lattice or fiber. Level 2: again a 40×1000 lattice composed by second level "springs," each of them identical to the entire fiber analyzed at the first level, is analyzed with the elastic modulus as input and stochastic strength distribution derived as the output of the numerous simulations to be carried out at the first level. And so on. Five hierarchical levels are sufficient to reach the size scale of the megameter from that of the nanometer (Fig. 18.1).

The Level 1 simulation is carried out with springs $L_0 = 10^{-7}$ m in length, $w_0 = 10^{-9}$ m in width, with Young's modulus $E_0 = 10^{12}$ Pa and strength σ_f randomly distributed according to the nanoscale Weibull statistics [16] $P(\sigma_f) = 1 - \exp[-(\sigma_f/\sigma_0)^m]$, where P is the cumulative probability. Fitting to the experiments on carbon nanotubes [7,8], we have derived for carbon nanotubes $\sigma_0 = 34$ GPa and $m = 2.7$ [16]. Then, Level 2 is computed, and so on. The results are summarized in Fig. 18.2, in which a strong size effect is observed, up to length of ~ 1 m.

Given the decaying σ_f vs cable length L obtained from simulations, it is interesting to fit the behavior with simple analytical scaling laws. Various laws exist in the literature, and one of the most used is the multifractal scaling law (MFSL [17,18]). This law has been recently extended toward the nanoscale [19]:

$$\frac{\sigma_f}{\sigma_{\text{macro}}} = \sqrt{1 + \frac{l_{\text{ch}}}{L + l_0}} \tag{18.1}$$

where σ_f is the failure stress, σ_{macro} is the macrostrength, L is the structural characteristic size, l_{ch} is the characteristic internal length and l_0 is defined via $\sigma_f(l = 0) = \sigma_{\text{macro}}\sqrt{1 + \dfrac{l_{\text{ch}}}{l_0}} \equiv \sigma_{\text{nano}}$, where σ_{nano} is the nanostrength. Note that
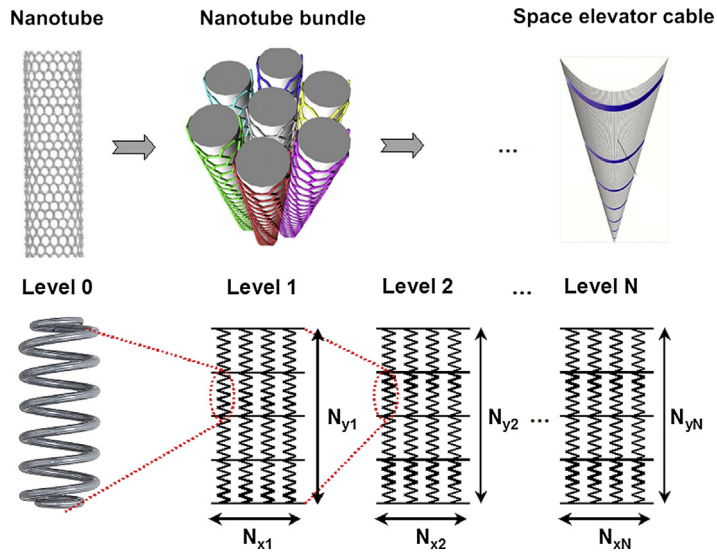
FIGURE 18.1

Schematization of the adopted multiscale simulation procedure to determine the space elevator cable strength. Here, $N = 5$, $N_{x1} = N_{x2} = \ldots N_{x5} = 40$ and $N_{y1} = N_{y2} = \ldots N_{y5} = 1000$, so that the total number of nanotubes or graphene ribbons in the space elevator cable is $N_{tot} = (1000 \times 40)^5 \approx 10^{23}$ [15] From: Multiscale stochastic simulations as in-silico tensile testing of nanotube-based megacables, Small 4, 2008. (For color version of this figure, the reader is referred to the online version of this book.)
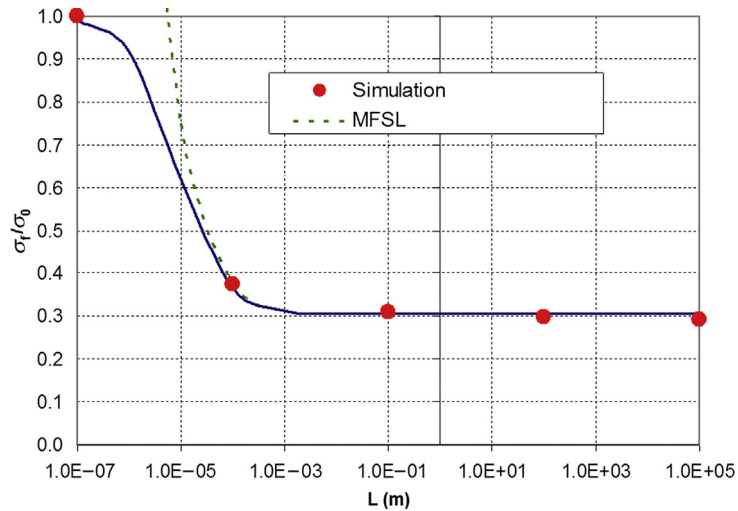
FIGURE 18.2

Comparison between simulations (dots) and analytical scaling law (Eqn (18.1)) for the failure strength of the nanotube bundle as a function of its length; the asymptote is at 10.20 GPa [15]. The dotted line corresponds to Co=o, thus to [17]. (For color version of this figure, the reader is referred to the online version of this book.)

for $l_0 = 0$, this law is that reported in [17]. Here, we can choose σ_{nano} as the nanotube stochastic strength, i.e. $\sigma_{nano} = 34$ GPa. The computed macrostrength is $\sigma_{macro} = 10.20$ GPa. The fit with Eqn (18.1) is shown in Fig. 18.1 for the various L considered at the different hierarchical levels. The best fit is obtained for $l_{ch} = 5 \times 10^{-5}$ m, where the analytical law is practically coincident with the simulated results. Thus, for a carbon nanotube or graphene megacable, we have numerically derived a plausible strength $\sigma_C = \sigma_{macro} \approx 10$ GPa.

18.3 BRITTLE FRACTURE

By considering QFM [11−14], the failure stress σ_N for a nanotube or graphene having atomic size q (the "fracture quantum") and containing an elliptical hole of half-axes a perpendicular to the applied load (or nanotube or graphene axis) and b can be determined including in the asymptotic solution [12] the contribution of the far-field stress. We accordingly derive

$$\frac{\sigma_N(a,b)}{\sigma_N^{(theo)}} = \sqrt{\frac{1 + 2a/q(1+2a/b)^{-2}}{1 + 2a/q}}, \quad \sigma_N^{(theo)} = \frac{K_{IC}}{\sqrt{q\pi/2}} \tag{18.2}$$

where $\sigma_N^{(theo)}$ is the theoretical (defect-free) nanotube or graphene strength (~ 100 GPa, see Table 18.1) and K_{IC} is the material fracture toughness. The self-interaction between the tips has been neglected here (i.e. $a \ll \pi R$, W with R the nanotube radius or W, the graphene width) and would further reduce the failure stress. For atomistic defects (having characteristic length of few Ångstrom) in nanotubes or graphene (having characteristic diameter of several nanometers), this hypothesis is fully verified. However, QFM can easily treat also the self-tip inter-action starting from the corresponding value of the stress-intensity factor (reported in the related handbooks). The validity of QFM has been recently confirmed by atomistic simulations [3−5,12,13,20], but also at larger size scales [12,13,21] and for fatigue crack growth [14,22,23].

Regarding the defect shape, for a sharp crack perpendicular to the applied load, $a/q = $ const and $b/q \to 0$; thus, $\sigma_N \approx \sigma_N^{(theo)}/\sqrt{1 + 2a/q}$, and for $a/q \gg 1$, i.e. large cracks, $\sigma_N \approx K_{IC}/\sqrt{\pi a}$ in agreement with linear elastic fracture mechanics (LEFM); note that LEFM can (1) only treat sharp cracks and (2) unreasonably predict an infin-ite defect-free strength. On the other hand, for a crack parallel to the applied load, $b/q = $ const and $a/q \to 0$, and thus, $\sigma_N = \sigma_N^{(theo)}$, as it must be. In addition, regarding the defect size, for self-similar and small holes, $a/b = $ const & $a/q \to 0$ and coherently $\sigma_N = \sigma_N^{(theo)}$; furthermore, for self-similar and large holes, $a/b = $ const & $a/q \to \infty$ and we deduce $\sigma_N \approx \sigma_N^{(theo)}/(1 + 2a/b)$ in agreement with the stress concentration posed by elasticity; but elasticity (coupled with a maximum stress crite-rion) unreasonably predicts (3) a strength independent from the hole size and (4) tending to zero for cracks. Note the extreme consistency of Eqn (18.2) that, removing all the

Table 18.1 Atomistic Simulations [30–34] vs QFM Predictions, for Nanocracks of Size *n* or Nanoholes of Size *m* in carbon nanotubes or graphene ribbons. (From: The role of defects in the design of the space elevator cable: from nanotube to megatube, Acta Materialia 55 2007) [4]

Graphene/ Nanotube Type	Nanocrack (*n*) and Nanohole (*m*) sizes	Strength [GPa] by QM (MTB-G2) and MM (PM3; M) QM/MM Atomistic or QFM Calculations
[5,5]	Defect-free	105 (MTB-G2); 135 (PM3)
[5,5]	$n = 1$ (Sym.+H)	85 (MTB-G2), 79 (QFM); 106 (PM3), 101 (QFM)
[5,5]	$n = 1$ (Asym. +H)	71 (MTB-G2), 79 (QFM); 99 (PM3), 101 (QFM)
[5,5]	$n = 1$ (Asym.)	70 (MTB-G2), 79 (QFM); 100 (PM3), 101 (QFM)
[5,5]	$n = 2$ (Sym.)	71 (MTB-G2), 63 (QFM); 105 (PM3), 81 (QFM)
[5,5]	$n = 2$ (Asym.)	73 (MTB-G2), 63 (QFM); 111 (PM3), 81 (QFM)
[5,5]	$m = 1$ (+H)	70 (MTB-G2), 68 for long tube, 79 (QFM); 101 (PM3), 101 (QFM)
[5,5]	$m = 2$ (+H)	53 (MTB-G2), 50 for long tube, 67 (QFM); 78 (PM3), 86 (QFM)
[10,10]	Defect-free	88 (MTB-G2); 124 (PM3)
[10,10]	$n = 1$ (Sym.+H)	65 (MTB-G2), 66 (QFM)
[10,10]	$n = 1$ (Asym. +H)	68 (MTB-G2), 66 (QFM)
[10,10]	$n = 1$ (Sym.)	65 (MTB-G2), 66 (QFM); 101 (PM3), 93 (QFM)
[10,10]	$n = 2$ (Sym.)	64 (MTB-G2), 53 (QFM); 107 (PM3), 74 (QFM)
[10,10]	$n = 2$ (Asym.)	65 (MTB-G2), 53 (QFM); 92 (PM3), 74 (QFM)
[10,10]	$m = 1$ (+H)	56 (MTB-G2), 52 for long tube, 66 (QFM); 89 (PM3), 93 (QFM)
[10,10]	$m = 2$ (+H)	42 (MTB-G2), 36 for long tube, 56 (QFM); 67 (PM3), 79 (QFM)
[50,0]	Defect-free	89 (MTB-G2)
[50,0]	$m = 1$ (+H)	58 (MTB-G2); 67 (QFM)
[50,0]	$m = 2$ (+H)	46 (MTB-G2); 57 (QFM)
[50,0]	$m = 3$ (+H)	40 (MTB-G2); 44 (QFM)
[50,0]	$m = 4$ (+H)	36 (MTB-G2); 41 (QFM)
[50,0]	$m = 5$ (+H)	33 (MTB-G2); 39 (QFM)
[50,0]	$m = 6$ (+H)	31 (MTB-G2); 37 (QFM)
[100,0]	Defect-free	89 (MTB-G2)
[100,0]	$m = 1$ (+H)	58 (MTB-G2); 67 (QFM)

Table 18.1 Atomistic Simulations [30–34] vs QFM Predictions, for Nanocracks of Size *n* or Nanoholes of Size *m* in carbon nanotubes or graphene ribbons. (From: The role of defects in the design of the space elevator cable: from nanotube to megatube, Acta Materialia 55 2007) [4]—Cont'd

Graphene/ Nanotube Type	Nanocrack (*n*) and Nanohole (*m*) sizes	Strength [GPa] by QM (MTB-G2) and MM (PM3; M) QM/MM Atomistic or QFM Calculations
[100,0]	$m = 2$ (+H)	47 (MTB-G2); 57 (QFM)
[100,0]	$m = 3$ (+H)	42 (MTB-G2); 44 (QFM)
[100,0]	$m = 4$ (+H)	39 (MTB-G2); 41 (QFM)
[100,0]	$m = 5$ (+H)	37 (MTB-G2); 39 (QFM)
[100,0]	$m = 6$ (+H)	35 (MTB-G2); 37 (QFM)
[29,29]	Defect-free	101 (MTB-G2)
[29,29]	$m = 1$ (+H)	77 (MTB-G2); 76 (QFM)
[29,29]	$m = 2$ (+H)	62 (MTB-G2); 65 (QFM)
[29,29]	$m = 3$ (+H)	54 (MTB-G2); 50 (QFM)
[29,29]	$m = 4$ (+H)	48 (MTB-G2); 46 (QFM)
[29,29]	$m = 5$ (+H)	45 (MTB-G2); 44 (QFM)
[29,29]	$m = 6$ (+H)	42 (MTB-G2); 42 (QFM)
[47,5]	Defect-free	89 (MTB-G2)
[47,5]	$m = 1$ (+H)	57 (MTB-G2); 67 (QFM)
[44,10]	Defect-free	89 (MTB-G2)
[44,10]	$m = 1$ (+H)	58 (MTB-G2); 67 (QFM)
[40,16]	Defect-free	92 (MTB-G2)
[40,16]	$m = 1$ (+H)	59 (MTB-G2); 69 (QFM)
[36,21]	Defect-free	96 (MTB-G2)
[36,21]	$m = 1$ (+H)	63 (MTB-G2); 72 (QFM)
[33,24]	Defect-free	99 (MTB-G2)
[33,24]	$m = 1$ (+H)	67 (MTB-G2); 74 (QFM)
[80, 0]	Defect-free	93 (M)
[80, 0]	$n = 2$	64 (M); 56 (QFM)
[80, 0]	$n = 4$	50 (M); 43 (QFM)
[80, 0]	$n = 6$	42 (M); 35 (QFM)
[80, 0]	$n = 8$	37 (M); 32 (QFM)
[40, 0] (nested by a [32, 0])	Defect-free	99 (M)
[40, 0] (nested by a [32, 0])	$n = 2$	73 (M); 69 (QFM + *vdW* interaction $\sim$10 GPa)
[40, 0] (nested by a [32, 0])	$n = 4$	57 (M); 56 (QFM + *vdW* interaction $\sim$10 GPa)
[40, 0] (nested by a [32, 0])	$n = 6$	50 (M); 48 (QFM + *vdW* interaction $\sim$10 GPa)
	$n = 8$	

Table 18.1 Atomistic Simulations [30–34] vs QFM Predictions, for Nanocracks of Size *n* or Nanoholes of Size *m* in carbon nanotubes or graphene ribbons. (From: The role of defects in the design of the space elevator cable: from nanotube to megatube, Acta Materialia 55 2007) [4]—Cont'd

Graphene/ Nanotube Type	Nanocrack (*n*) and Nanohole (*m*) sizes	Strength [GPa] by QM (MTB-G2) and MM (PM3; M) QM/MM Atomistic or QFM Calculations
[40, 0] (nested by a [32, 0])		44 (M); 44 (QFM + *vdW* interaction ~10 GPa)
[100,0]	Defect-free	89 (MTB-G2)
[100,0]	*n* = 4	50 (M); 41 (QFM)
[10,0]	Defect free	124 (QM); 88 (MM);
[10,0]	*n* = 1	101 (QM) 95 (QM/MM) 93 (QFM); 65 (MM) 66 (QFM)

The QFM predictions are here obtained simply considering in Eqn (18.2) 2a/q = n, 2b/q = 1 for cracks of size n or a/q = b/q = (2m − 1)/√3 for holes of size m. Quantum mechanics (QM) semiempirical calculations (PM3 method), molecular mechanics (MM) calculations (modified Tersoff–Brenner potential of second generation (MTB-G2), modified Morse potential (M)) and coupled QM/MM calculations. The symbol (+H) means that the defect was saturated with hydrogen. Symmetric and asymmetric bond reconstructions were also considered; the tubes are "short", if not otherwise specified. We have roughly ignored in the QFM predictions the difference between symmetric and asymmetric bond reconstruction, hydrogen saturation and length effect (for shorter tubes, an increment in the strength is always observed as an intrinsic size effect), noting that the main differences in the atomistic simulations are imputable to the used potential. For nested nanotubes, a strength increment of ~10 GPa is here assumed to roughly take into account the van der Walls (vdW) interaction between the walls.

limitations (1−4) represents the first law capable of describing in a unified manner all the size and shape effects for the elliptical holes, including cracks as limit case. In other words, Eqn (18.2) shows that the two classical strength predictions based on stress intensifications (LEFM) or stress concentrations (elasticity) are only reasonable for "large" defects; Eqn (18.2) unifies their results and extends its validity to "small" defects ("large" and "small" are here with respect to the fracture quantum). Equation (18.2) shows that even a small defect can dramatically reduce the mechanical strength.

An upper bound of the cable strength can be derived assuming the simultaneous failure of all the defective nanotubes or graphene layers present in the bundle. Accordingly, imposing the critical force equilibrium (mean-field approach) for a cable composed of nanotubes or graphene layers in numerical fractions f_{ab} containing holes of half-axes *a* and *b*, we find the cable strength σ_C (ideal if $\sigma_C^{(\text{theo})}$) in the following form:

$$\frac{\sigma_C}{\sigma_C^{(\text{theo})}} = \sum_{a,b} f_{ab} \; \frac{\sigma_N(a,b)}{\sigma_N^{(\text{theo})}} \tag{18.3}$$

The summation is extended to all the different holes; the numerical fraction f_{00} of nanotubes/graphene is defect-free and $\sum_{a,b} f_{ab} = 1$. If all the defective

nanotubes/graphene in the bundle contain identical holes $f_{ab} = f = 1 - f_{00}$, and the following simple relation between the strength reductions holds: $1 - \sigma_C / \sigma_C^{(theo)} = f(1 - \sigma_N / \sigma_N^{(theo)})$.

Thus, the taper ratio λ needed to have a uniform stress in a space elevator cable [2], under the centrifugal and gravitational forces, must be larger than its theoretical value, in order to design a flaw-tolerant megacable. In fact, according to our analysis, we deduce ($\lambda = e^{const.\rho_C / \sigma_C} \geq \lambda^{(theo)} \approx 1.9$ for carbon nanotubes/graphene; ρ_C denotes the material density) the following:

$$\frac{\lambda}{\lambda^{(theo)}} = \lambda^{(theo)\left(\frac{\sigma_C^{(theo)}}{\sigma_c} - 1\right)} \tag{18.4}$$

Equation (18.4) shows that a small defect can dramatically increase the taper ratio required for a flaw-tolerant megacable and thus, nearly proportionally, its mass.

18.4 ELASTIC-PLASTICITY, FRACTAL CRACKS AND FINITE DOMAINS

The previous equations are based on linear elasticity, i.e. on a linear relationship $\sigma \propto \varepsilon$ between stress σ and strain ε. In contrast, let us assume $\sigma \propto \varepsilon^\kappa$, where $\kappa > 1$ denotes hyperelasticity, as well as $\kappa < 1$ denotes elastic-plasticity. The power of the stress singularity will accordingly be modified [24] from the classical value $1/2$ to $\alpha = \kappa/(\kappa + 1)$. Thus, the problem is mathematically equivalent to that of a reentrant corner [25], and consequently, we predict

$$\frac{\sigma_N(a,b,\alpha)}{\sigma_N^{(theo)}} = \left(\frac{\sigma_N(a,b)}{\sigma_N^{(theo)}}\right)^{2\alpha}, \quad \alpha = \frac{\kappa}{\kappa + 1} \tag{18.5}$$

A crack with a self-similar roughness, mathematically described by a fractal with noninteger dimension $1 < D < 2$, would similarly modify the stress singularity, according to $\alpha = (2 - D)/2$ [18,26]; thus, with Eqn (18.5), we can also estimate the role of the crack roughness. Both plasticity and roughness reduce the severity of the defect, whereas hyperelasticity enlarges its effect. For example, for a crack composed by n adjacent vacancies, we found $\sigma_N / \sigma_N^{(theo)} \approx (1 + n)^{-\alpha}$.

However, note that among these three effects, only elastic-plasticity may have a significant role in carbon nanotubes/graphene; in spite of this, fractal cracks could play an important role in nanotube/graphene bundles as a consequence of their larger size scale, which would allow the development of a crack surface roughness. Hyperelasticity is not expected to be relevant in this context (but important for biological materials such as spider silk).

According to LEFM and assuming the classical hypothesis of self-similarity ($a_{max} \propto L$), i.e. the largest crack size is proportional to the characteristic structural

size L, we expect a size effect on the strength in the form of the power law $\sigma_C \propto L^{-\alpha}$. For linear elastic materials, $\alpha = 1/2$ as classically considered, but for elastic-plastic materials or fractal cracks, $0 \le \alpha \le 1/2$ [24], whereas for hyperelastic materials, $1/2 \le \alpha \le 1$, suggesting an unusual and stronger size effect. This parameter would represent the maximum slope (in a bi-log plot) of the scaling as reported in Fig. 18.1.

Equation (18.2) does not consider the defect–boundary interaction. The finite width $2W$ can be treated by applying QFM starting from the related expression of the stress-intensity factor (reported in handbooks). However, to have an idea of the defect–boundary interaction, we apply an approximated method [27], deriving the following correction $\sigma_N(a,b,W) \approx C(W)\sigma_N(a,b)$, $C(W) \approx (1 - a/W)/$ $(\sigma_N(a,b)|_{q \to W-a}/\sigma_N^{(\text{theo})})$ (note that such a correction is valid also for $W \approx a$, whereas for $W \gg a$, it becomes $C(W \gg a) \approx 1 - a/W$). Similarly, the role of the defect orientation β could be treated by QFM considering the related stress-intensity factor; roughly, one could use the self-consistent approximation $\sigma_N(a,b,\beta) \approx \sigma_N(a,b)\cos^2\beta + \sigma_N(b,a)\sin^2\beta$.

18.5 FATIGUE

The superstrong fibers can be cyclically loaded, e.g. in a space elevator cable by the climbers carrying the payloads, thus fatigue could play a role on their design. By integrating the quantized Paris' law, that is an extension of the classical Paris' law recently proposed especially for nanostructure or nanomaterial applications [14,22,23], we derive the following number of cycles to failure (or life time):

$$\frac{C_N(a)}{C_N^{(\text{theo})}} = \frac{(1 + q/W)^{1-m/2} - (a/W + q/W)^{1-m/2}}{(1 + q/W)^{1-m/2} - (q/W)^{1-m/2}}, \quad m \ne 2 \tag{18.6a}$$

$$\frac{C_N(a)}{C_N^{(\text{theo})}} = \frac{\ln[(1 + q/W)/(a/W + q/W)]}{\ln[(1 + q/W)/(q/W)]}, \quad m = 2 \tag{18.6b}$$

where $m>0$ is the material Paris' exponent. Note that according to Wöhler, $C_N^{(\text{theo})} = K\Delta\sigma^{-k}$, where K and k are material constants and $\Delta\sigma$ is the amplitude of the stress range during the oscillations. Even if fatigue experiments in nanotubes/graphene are still to be performed, their behavior is expected to be intermediate between those of Wöhler and Paris, as displayed by all the known materials, and the quantized Paris' law basically represents their asymptotic matching (as QFM basically represents the asymptotic matching between the strength and toughness approaches).

Only defects remaining self-similar during fatigue growth have to be considered, thus only a crack (of half-length a) is of interest in this context. By means of Eqn (18.6), the time to failure reduction can be estimated, similarly to the brittle fracture treated by Eqn (18.2).

For a bundle, considering a mean-field approach (similarly to Eqn (18.3)) yields

$$\frac{C_C}{C_C^{(\text{theo})}} = \sum_a f_a \frac{C_N(a)}{C_N^{(\text{theo})}} \tag{18.7}$$

Better predictions could be derived integrating the quantized Paris' law for a finite width strip. However, we note that the role of the finite width is already included in Eqn (18.6), even if these are rigorously valid in the limit of W tending to infinity.

18.6 ELASTICITY

Consider a nanotube/graphene of lateral surface A under tension and containing a transversal crack of half-length a. Interpreting the incremental compliance, due to the presence of the crack, as a Young's modulus (here denoted by E) degradation, we find $\frac{E(a)}{E^{(\text{theo})}} = 1 - 2\pi\frac{a^2}{A}$ [28]. Thus, recursively, considering Q cracks (in the megacable, $10^{12}-10^{20}$ defects are expected, see Section 2) having sizes a_i or, equivalently, M different cracks with multiplicity Q_i ($Q = \sum_{i=1}^{M} Q_i$), noting that $n_i = \frac{2a_i}{q}$ represents the number of adjacent vacancies in a crack of half-length a_i, with q atomic size, and $v_i = \frac{Q_i n_i}{A/q^2}$ its related numerical (or volumetric) vacancy fraction, we find [28]

$$\frac{E}{E^{(\text{theo})}} = \prod_{i=1}^{Q} \frac{E(a_i)}{E^{(\text{theo})}} \approx 1 - \xi \sum_{i=1}^{M} v_i n_i \tag{18.8}$$

with $\xi \geq \pi/2$, where the equality holds for isolated cracks. Equation (18.8) can be applied to nanotubes or graphene and related bundles containing defects in volumetric percentages v_i.

Forcing the interpretation of our formalism, we note that $n_i = 1$ would describe a single vacancy, i.e. a small hole. Thus, as a first approximation, different defect geometries from cracks to circular holes, e.g. elliptical holes, could in principle be treated by Eqn (18.8); we have to interpret n_i as the ratio between the transversal and longitudinal (parallel to the load) defect sizes ($n_i = a_i/b_i$). Introducing the i-th defect eccentricity e_i as the ratio between the lengths of the longer and shorter axes, as a first approximation, $n_i(\beta_i) \approx e_i \cos^2\beta_i + 1/e_i \sin^2\beta_i$, where β_i is the defect orientation. For a single-defect typology, $\frac{E}{E^{(\text{theo})}} \approx 1 - \xi v n$, in contrast to the common assumption $\frac{E}{E^{(\text{theo})}} \approx 1 - v$, rigorously valid only for the cable density, for which $\frac{\rho_C}{\rho_C^{(\text{theo})}} \equiv 1 - v$. Note that the failure strain for a defective nanotube, graphene or related bundle can also be predicted by $\varepsilon_{N,C}/\varepsilon_{N,C}^{(\text{theo})} = (\sigma_{N,C}/\sigma_{N,C}^{(\text{theo})})/(E/E^{(\text{theo})})$.

In contrast to what happens for the strength, large defectiveness is required to have a considerable elastic degradation, even if we have shown that sharp transversal defects could have a role. For example, too-soft space elevator cables would become dynamically unstable [29].

18.7 ATOMISTIC SIMULATIONS

Let us study the influence on the strength of nanocracks and circular nanoholes. n atomic adjacent vacancies perpendicular to the load correspond to a blunt nanocrack of length $2a \approx nq$ and thickness $2b \approx q$ (or $2a \approx nq$ with a radius at tips of $b^2/a \approx q/2$). Similarly, nanoholes of size m can be considered: the index $m = 1$ corresponds to the removal of an entire hexagonal ring, $m = 2$ to the additional removal of the six hexagons around the former one (i.e. the adjacent perimeter of 18 atoms), $m = 3$ to the additional removal of the neighboring 12 hexagonal rings (next adjacent perimeter), and so on (thus, $a = b \approx q(2m - 1)/\sqrt{3}$). Quantum mechanics (QM), semiempirical (PM3 method), molecular mechanics (MM; with a modified Tersoff—Brenner potential of second generation (MTB-G2) or a modified Morse potential (M)) and coupled QM/MM calculations [30—34] are reported and extensively compared in Table 18.1 with the QFM nonasymptotic predictions of Eqn (18.2) (differently from the asymptotic comparison reported in Refs [3,12]). The comparison shows a relevant agreement, confirming and demonstrating that just a few vacancies can dramatically reduce the strength of a single nanotube/graphene, or of a nanotube/graphene bundle as described by Eqn (18.3) that predicts for $f \approx 1$, $\sigma_C/\sigma_C^{(theo)} \approx \sigma_N/\sigma_N^{(theo)}$. Assuming large holes ($m \to \infty$) and applying QFM to a defective bundle ($f \approx 1$), we predict $1 - \sigma_C/\sigma_C^{(theo)} \approx 1 - \sigma_N/\sigma_N^{(theo)} \approx 67\%$; but nanocracks surely would be even more critical, especially if interacting with each other or with the boundary. Thus, the expectation for a nanotube/graphene megacable of strength larger than ~ 33 GPa is unlikely.

Note that an elastic ($\kappa \approx 1$), nearly perfectly plastic ($\kappa \approx 0$) behavior with a flow stress at ~ 30—35 GPa for strains larger than ~ 3—5% has been recently observed in tensile tests of carbon nanotubes [35], globally suggesting $\kappa \approx 0.6$—0.7; similarly, numerically computed stress—strain curves [36] reveal for an armchair (5,5) carbon nanotube $\kappa \approx 0.8$, whereas for a zigzag (9,0) nanotube $\kappa \approx 0.7$, suggesting that the plastic correction reported in Section 4 could have a role in nanotubes or graphene.

Regarding elasticity, we note that Eqn (18.8) can be viewed as a generalization of the approach proposed in Ref. [37], being able to quantify the constants k_i fitted by atomistic simulations for three different types of defect [28]. In particular, rearranging Eqn (18.8) and in the limit of three small cracks, we deduce $\frac{E_{th}}{E} \approx 1 + k_1 c_1 + k_2 c_2 + k_3 c_3$, identical to their law (Eqn (18.15)), in which $c_i = Q_i/L$ is the linear defect concentration in a nanotube of length L and radius R and $k_i = \frac{\xi c_i n_i^2 q^2}{\pi^2 R}$. These authors consider 1, 2 and 3 atoms missing, with and without

reconstructed bonds; for nonreconstructed bonds two alternative defect orientations were investigated for 2 and 3 atoms missing. Even if their defect geometries are much more complex than the nanocracks that we consider here, the comparison between our approach and their atomistic simulations, which does not involve best-fit parameters, shows a good agreement [28].

18.8 NANOTENSILE TESTS

The discussed tremendous defect sensitivity, described by Eqn (18.2), is confirmed by a statistical analysis based on Nanoscale Weibull Statistics (NWS) [16] applied to nanotensile tests. According to this treatment, the probability of failure P for a nearly defect-free nanotube/graphene under a tensile stress σ_N is independent from its volume (or surface), in contrast to classical Weibull Statistics [38], namely,

$$P = 1 - \exp - N_N \left(\frac{\sigma_N}{\sigma_0}\right)^w \tag{18.9}$$

where w is the nanoscale Weibull modulus, σ_0 is the nominal failure stress (i.e. corresponding to a probability of failure of 63%) and $N_N \equiv 1$. In classical Weibull statistics, $N_N \equiv V/V_0$ for volume dominating defects (or $N_N = A/A_0$ for surface dominating defects), i.e. N_N is the ratio between the volume (or surface) of the structure and a reference volume (or surface). The experimental data on carbon nanotubes [7,8] were treated [16] according to nanoscale and classical Weibull statistics: the coefficients of correlation were found to be much higher for the nanoscale statistics than for the classical one (0.93 against 0.67, $w \approx 2.7$ and $\sigma_0 \approx 31-34$ GPa). The data set on MWCNT tensile experiments [39] has also been statistically treated [3]. The very large, highest measured strengths denote interactions between the external and internal walls, as pointed out by the same authors [39] and recently quantified [14]. Thus, the measured strengths cannot be considered plausible for describing the strength of a SWCNT. Such experiments were best-fitted with $\sigma_0 \approx 108$ GPa (but not significant for the strength of a single nanotube) and $w \approx 1.8$ (coefficient of correlation 0.94). In Fig. 18.3, the new data set [40] is treated [4] by applying NWS ($N_N \equiv 1$, $w \approx 2.2$, $\sigma_0 \approx 25$ GPa) and compared with the other nanoscale statistics [3,4] deduced from the other data sets [7,8,39]. Note that volume- or surface-based Weibull statistics are identical in treating the external wall of the tested nanotubes, just an atomic layer thick. We have found a poor coefficient of correlation also treating this new data set with classical Weibull statistics, namely 0.51 (against 0.88 for NWS, see Fig. 18.3).

All these experimental data [7,8,39,40] are treated in Table 18.2, by applying QFM in the form of Eqn (18.2): nonlinear multiple solutions for identifying the defects corresponding to the measured strength clearly emerge; however, these are quantifiable, showing that a small defect is sufficient to rationalize the majority of the observed strong strength reductions.
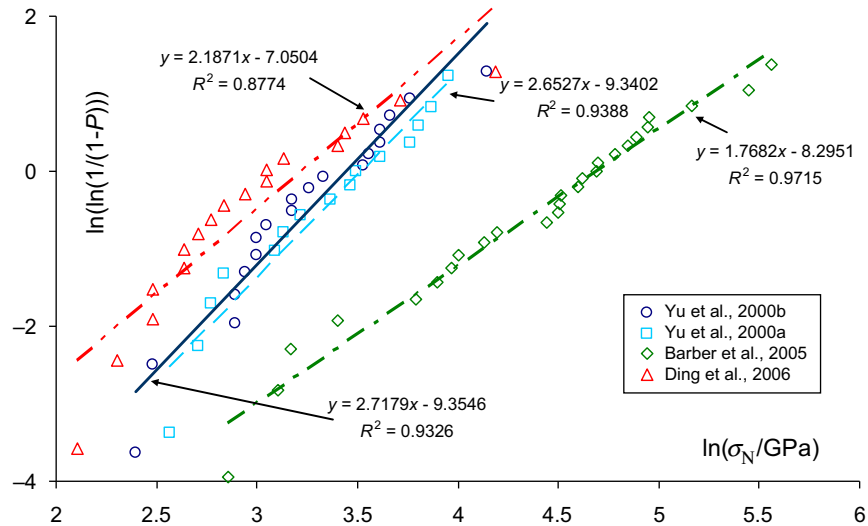
FIGURE 18.3

Nanoscale Weibull statistics, straight lines, applied to nanotensile experiments on carbon nanotubes. From: The role of defects in the design of the space elevator cable: from nanotube to megatube, Acta Materialia 55 2007 [4]. (For color version of this figure, the reader is referred to the online version of this book.)

Finally, the new experimental results [39] are differently treated in Table 18.3, with respect to both strength and elasticity, assuming the presence of transversal nanocracks. The ideal strength is assumed to be of 100 GPa and the theoretical Young's modulus of 1 TPa; by Eqn (18.2), the crack length n is calculated and introduced in Eqn (18.8) to derive the related vacancy fraction v ($\xi = \pi/2$).

18.9 THERMODYNAMIC LIMIT

Defects are thermodynamically unavoidable, especially at the megascale. At the thermal equilibrium, the vacancy fraction $f = n/N \ll 1$ (n is the number of vacancies and N is the total number of atoms) is estimated as follows [41]:

$$f \approx e^{-E_1(k_B T_a)} \tag{18.10}$$

where $E_1 \approx 7$ eV is the energy required to remove one carbon atom and T_a is the absolute temperature at which the carbon is assembled, typically in the range between 2000 and 4000 K. Thus, $f \approx 2.4 \times 10^{-18} - 1.6 \times 10^{-9}$. For example for a space elevator megacable, having a carbon weight of ~ 5000 Kg, the total number of atoms is $N \approx 2.5 \times 10^{29}$, thus a huge number of equilibrium defects in the range $n \approx 0.6 \times 10^{12} - 3.9 \times 10^{20}$ is expected in agreement with a recent discussion [42] and observations [43].

Table 18.2 Experiments vs QFM Predictions; Strength Reduction $\sigma_N(a,b)/\sigma_N^{(theo)}$ Derived According to Eqn (18.2) for carbon nanotubes and graphene. From: The role of defects in the design of the space elevator cable: from nanotube to megatube, Acta Materialia 55 2007 [4]

$\sigma_N/\sigma_N^{(theo)}$	2a/q	2b/q	0	1	2	3	4	5	6	7	8	9	10	∞
0			1.00*	1.00*	1.00*	1.00*	1.00*	1.00*	1.00*	1.00*	1.00*	1.00*	1.00*	1.00
1			0.71*	0.75	0.79	0.82	0.85	0.87*	0.88*	0.90	0.91	0.91	0.92	1.00
2			0.58	0.60*	0.64*	0.68	0.71*	0.73	0.76	0.78*	0.79	0.81	0.82	1.00
3			0.50	**0.52**	0.54*	0.58	0.61	0.64*	<u>0.66*</u>	0.68	0.70*	0.72	0.74	1.00
4			**0.45**	0.46	**0.48**	0.51*	0.54*	0.56	0.59	0.61	*0.63*	0.65	0.67	1.00
5			<u>0.41</u>	0.42	0.44*	0.46	**0.48**	0.51*	0.53*	0.55*	0.58	0.59	0.61	1.00
6			0.38	0.38	0.40	0.42	0.44*	0.47	0.49*	0.51*	0.53*	0.55*	0.57	1.00
7			*0.35*	0.36	***0.37***	*0.39*	<u>0.41</u>	***0.43***	**0.45**	0.47	0.49*	0.51*	0.53*	1.00
8			**0.33**	<u>0.34</u>	*0.35*	***0.37***	0.38	0.40	0.42	0.44*	0.46	**0.48**	0.49*	1.00
9			**0.32**	**0.32**	**0.33**	<u>0.34</u>	0.36	0.38	0.40	<u>0.41</u>	***0.43***	**0.45**	0.46	1.00
10			<u>0.30*</u>	<u>0.30*</u>	0.31	**0.33**	*0.34*	0.36	***0.37***	0.39	<u>0.41</u>	0.42	0.44*	1.00
11			**0.29**	**0.29**	0.30*	0.31	**0.32**	*0.34*	*0.35*	**0.37**	0.39	0.40	0.42	1.00
12			*0.28*	*0.28*	**0.29**	0.30*	*0.31*	**0.32**	*0.34*	***0.37***	0.38	0.40	1.00
13			0.27	0.27	*0.28*	**0.29**	0.30*	*0.31*	**0.32**	<u>0.34</u>	0.35	0.36	0.38	1.00
14			*0.26*	*0.26*	0.27	0.27	**0.29**	0.30*	*0.31*	**0.32**	<u>0.34</u>	*0.35*	0.36	1.00
15			**0.25**	**0.25**	*0.26*	0.27	0.27	**0.29**	0.30*	0.31	**0.32**	<u>0.34</u>	*0.35*	1.00
16			*0.24**	*0.24**	**0.25**	*0.26*	0.27	*0.28*	**0.29**	0.30*	0.31	0.32	**0.33**	1.00
17			*0.24**	*0.24**	*0.24**	**0.25**	*0.26*	0.27	*0.28*	**0.29**	0.30*	0.31	**0.32**	1.00
18			<u>**0.23**</u>	<u>**0.23**</u>	*0.24**	*0.24**	**0.25**	*0.26*	0.27	*0.28*	**0.29**	0.30*	<u>0.31</u>	1.00
19			**0.22***	**0.22***	**0.23**	0.23	*0.24**	**0.25**	*0.26*	0.27	*0.28*	**0.29**	<u>0.30*</u>	1.00
20			**0.22***	**0.22***	**0.22***	<u>0.23</u>	*0.24**	*0.24**	**0.25**	0.26	0.27	*0.28*	**0.29**	1.00
21			<u>*0.21*</u>	<u>*0.21*</u>	**0.22***	**0.22***	<u>0.23</u>	*0.24**	**0.25**	**0.25**	*0.26*	0.27	*0.28*	1.00

(*Continued*)

Table 18.2 Experiments vs QFM Predictions; Strength Reduction $\sigma_N(a,b)/\sigma_N^{(theo)}$ Derived According to Eqn (18.2) for carbon nanotubes and graphene. From: The role of defects in the design of the space elevator cable: from nanotube to megatube, Acta Materialia 55 2007 [4]—Cont'd

$\sigma_N/\sigma_N^{(theo)}$	2a/q	2b/q	0	1	2	3	4	5	6	7	8	9	10	∞
22			0.21	0.21	0.21	0.22*	0.22*	0.23	0.24*	0.25	0.26	0.27	0.28	1.00
23			0.20	0.21	0.21	0.21	0.22*	0.23	0.23	0.24*	0.25	0.26	0.27	1.00
24			0.20	0.20	0.20	0.21	0.21	0.22*	0.23	0.24*	0.24*	0.25	0.26	1.00
25			0.20	0.20	0.20	0.20	0.21	0.22*	0.22*	0.23	0.24*	0.25	0.26	1.00
26			0.19	0.19	0.20	0.20	0.20	0.21	0.22*	0.22*	0.23	0.24*	0.25	1.00
27			0.19	0.19	0.19	0.20	0.20	0.21	0.21	0.22*	0.23	0.24*	0.24*	1.00
28			0.19	0.19	0.19	0.19	0.20	0.20	0.21	0.22*	0.22*	0.23	0.24*	1.00
29			0.18	0.18	0.19	0.19	0.19	0.20	0.20	0.21	0.22*	0.23	0.23	1.00
30			0.18	0.18	0.18	0.19	0.19	0.19	0.20	0.21	0.21	0.22*	0.23	1.00
31			0.18	0.18	0.18	0.18	0.19	0.19	0.20	0.20	0.21	0.22*	0.22*	1.00
32			0.17*	0.17*	0.18	0.18	0.18	0.19	0.19	0.20	0.21	0.21	0.22*	1.00
33			0.17*	0.17*	0.17*	0.18	0.18	0.19	0.19	0.20	0.20	0.21	0.21	1.00
34			0.17*	0.17*	0.17*	0.17*	0.18	0.18	0.19	0.19	0.20	0.20	0.21	1.00
35			0.17*	0.17*	0.17*	0.17*	0.17*	0.18	0.18	0.19	0.19	0.20	0.21	1.00
36			0.16	0.16	0.17*	0.17*	0.17*	0.18	0.18	0.19	0.19	0.20	0.20	1.00
37			0.16	0.16	0.16	0.17*	0.17*	0.17*	0.18	0.18	0.19	0.19	0.20	1.00
38			0.16	0.16	0.16	0.16	0.17*	0.17*	0.18	0.18	0.19	0.19	0.20	1.00
39			0.16	0.16	0.16	0.16	0.17*	0.17*	0.17*	0.18	0.18	0.19	0.19	1.00

40	**0.16**	**0.16**	**0.16**	**0.16**	**0.16**	**0.17***	**0.17***	*0.18*	*0.18*	*0.19*	*0.19*	1.00
41	**0.15**	**0.15**	**0.16**	**0.16**	**0.16**	**0.16**	**0.17***	**0.17***	*0.18*	*0.18*	*0.19*	1.00
42	**0.15**	**0.15**	**0.15**	**0.16**	**0.16**	**0.16**	**0.17***	**0.17***	*0.18*	*0.18*	*0.19*	1.00
43	**0.15**	**0.15**	**0.15**	**0.15**	**0.16**	**0.16**	**0.16**	**0.17***	**0.17***	*0.18*	*0.18*	1.00
44	**0.15**	**0.15**	**0.15**	**0.15**	**0.16**	**0.16**	**0.16**	**0.17***	**0.17***	*0.18*	*0.18*	1.00
45	**0.15**	**0.15**	**0.15**	**0.15**	**0.15**	**0.16**	**0.16**	**0.16**	**0.17***	**0.17***	*0.18*	1.00
46	**0.15**	**0.15**	**0.15**	**0.15**	**0.15**	**0.15**	**0.16**	**0.16**	**0.17***	**0.17***	*0.18*	1.00
47	0.14	0.14	**0.15**	**0.15**	**0.15**	**0.15**	**0.16**	**0.16**	**0.16**	**0.17***	**0.17***	1.00
48	0.14	0.14	0.14	**0.15**	**0.15**	**0.15**	**0.15**	**0.16**	**0.16**	**0.17***	**0.17***	1.00
49	0.14	0.14	0.14	0.14	**0.15**	**0.15**	**0.15**	**0.16**	**0.16**	**0.16**	**0.17***	1.00
50	0.14	0.14	0.14	0.14	**0.15**	**0.15**	**0.15**	**0.15**	**0.16**	**0.16**	**0.17***	1.00
∞	0.00	0.00	0.00	0.00	0.00	0.00	0.00	0.00	0.00	0.00	0.00	$(1+2a/b)^{-1}$

*In **bold** type are represented the 15 different nanostrengths measured on single-walled carbon nanotubes in bundle [7]; whereas in italic, we report the 19 nano-strengths measured on multiwalled carbon nanotubes [8], and in underlined type, the most recent 18 observations [35]. All the data are reported with the exception of the five smallest values of 0.08, 0.10 [35], 0.11 [8], 0.12 [8,35] and 0.13 [7], for which we would need for example adjacent vacancies (2b/q ∼ 1) in number n = 2a/q = 138–176, 90–109, 75–89, 64–74 and 55–63 respectively. The 26 strengths measured in Ref. [39] are also treated (asterisks), simply assuming two interacting walls for $100 < \sigma_N^{(exp)} \leq 200$ Gpa (thus, $\sigma_N = \sigma_N^{(exp)}/2$) or three interacting walls for $200 < \sigma_N^{(exp)} \leq 300$ Gpa($\sigma_N = \sigma_N^{(exp)}/3$). All the experiments are referred to $\sigma_N^{(theo)} = 100$ GPa (q ∼ 0.25 nm). If all the nanotubes in the cable contain identical holes, $\sigma_C/\sigma_C^{(theo)} = \sigma_N/\sigma_N^{(theo)}$.*

Table 18.3 Fracture strength, Young's modulus, non-linear elasticity, crack size and defect content estimations from Modulus nanotensile tests. From: Modulus, fracture strength, and brittle vs plastic response of the outer shell of arc-grown multiwalled carbon nanotubes, Experimental Mechanics 47 2006 [35]

MWCNT Number and Fracture Typology	Strength [GPa]	Young's Modulus [GPa]	κ	n	v (%)
1 (multiple load A)	8.2	1100	1.01	148	0.07
2 (clamp failed)	10	840	0.98	100	0.23
3	12	680	1.00	69	0.44
4 (failure at the clamp)	12	730	0.98	69	0.40
5 (multiple load B)	14	1150	1.02	51	0.14
6 (multiple load a)	14	650	0.97	51	0.62
7	15	1200	1.05	44	0.11
8	16	1200	1.02	39	0.13
9	17	960	1.00	34	0.49
10	19	890	0.97	27	0.74
11 (multiple load b)	21	620	0.99	22	1.51
12 (multiple load I)	21	1200	0.99	22	0.22
13 (multiple load II)	23	1250	0.99	18	0.17
14	30	870	1.00	11	1.92
15 (plasticity observed)	31	1200	0.59 (0.99)	10	0.49
16 (plasticity observed)	34	680	0.69 (1.02)	8	3.80
17 (multiple load III)	41	1230	1.03	5	0.69
18 (failure at the clamp)	66	1100	0.98	2	4.90

The new results [35] are here treated with respect to both strength and elasticity, assuming the presence of transversal nanocracks composed by n adjacent vacancies [4]. The constitutive parameter κ has been estimated as $\kappa \approx \ln(\varepsilon_N)/\ln(\sigma_N/E)$ for all the tests: note the low values for the two nanotubes that revealed plasticity (in brackets, the values calculated up to the incipient plastic flow are also reported). The ideal strength is assumed to be of 100 GPa and the theoretical Young's modulus of 1300 GPa; by Eqn (18.2), the crack length n is calculated and introduced in Eqn (18.8) to derive the related vacancy fraction v ($\xi = \pi/2$). Fracture in two cases was observed at the clamp; in one case, the clamp itself failed, thus the deduced strength represents a lower bound of the nanotube strength. Three nanotubes were multiple loaded (in two a,b and A,B or in three I,II, and III steps), i.e. after the breaking in two pieces of a nanotube, one of the two pieces was again tested and fractured at a higher stress. Two nanotubes displayed a plastic flow. A vacancy fraction of the order of few %₀ is estimated, suggesting that such nanotubes are much more defective than as imposed by the thermodynamic equilibrium, even if the defects are small and isolated. However, note that other interpretations are still possible, e.g. assuming the nanotubes coated by an oxide layer and rationalizing the ratio between the observed Young's modulus and its theoretical value as the volumetric fraction (for softer coating layers) of carbon in the composite structure.

The strength of the cable will be dictated by the largest transversal crack on it, according to the weakest link concept. The probability of finding a nanocrack of size m in a bundle with vacancy fraction f is $P(m) = (1 - f)f^m$, and thus, the number M of such nanocracks in a bundle composed by N atoms is $M(m) = P(m)N$. The size

of the largest nanocrack, which typically occurs once, is found from the solution to the equation $M(m) \approx 1$, which implies [44]:

$$m \approx -\ln[(1-f)N]/\ln f \approx -\ln N/\ln f \qquad (18.11)$$

For example, we deduce a size $m \approx 2-4$ for the largest thermodynamically unavoidable defect in the considered megacable. Inserting Eqns (18.11) and (18.10) into Eqn (18.2) evaluated for a transversal crack ($b \approx 0$ and $2a/q \approx m$), we deduce the statistical counterpart of Eqn (18.2) and thus, the following thermo-dynamical maximum achievable strength:

$$\frac{\sigma_N(N)}{\sigma_N^{(theo)}} \leq \frac{\sigma_N^{(max)}(N)}{\sigma_N^{(theo)}} = \frac{1}{\sqrt{1 + \dfrac{k_B T_a}{E_1} \ln N}} \qquad (18.12)$$

Then, inserting Eqn (18.12) into Eqns (18.3) and (18.4), the maximum cable strength and minimum taper ratio can be statistically deduced. The corresponding maximum achievable strength, at unavoidable limit (at least at the thermodynamic equilibrium), is ~ 45 GPa and the corresponding flaw-tolerant taper ratio is ~ 4.6. But the larger taper ratio implies a large cable mass and thus a large number N of atoms. Updating N in our statistical calculation yields the same, thus self-consistent, predictions. Statistically, we expect an even smaller strength, as previously discussed.

18.10 SLIDING FAILURE

The fracture mechanics approach could be of interest to evaluate the strength of nanotube/graphene bundles assuming a sliding failure mode [45]. This hypothesis is complementary to that of intrinsic nanotube/graphene fracture, already treated in the previous sessions. Thus we assume the interactions between adjacent nanotubes/graphene as the weakest links, i.e. that the fracture of the bundle composite is caused by nanotube sliding rather than by their intrinsic fracture.

Accordingly, the energy balance during a longitudinal delamination (here "delamination" has the meaning of Mode II crack propagation at the interface between adjacent nanotubes/graphene ribbons) dz under the applied force F is

$$d\Phi - F du - 2\gamma(P_C + P_{vdW})dz = 0 \qquad (18.13)$$

where $d\Phi$ and du are the strain energy and elastic displacement variation, respectively, due to the infinitesimal increment in the compliance caused by the delamination dz; P_{vdw} describes the still existing van der Waals attraction (e.g. attractive part of the Lennard-Jones potential) for vanishing nominal contact nanotube perimeter $P_C = 6a$ (the shear force between two nanotube/graphene layers becomes zero for nominally negative contact area); γ is the surface energy of the interface.

Elasticity poses $\dfrac{\mathrm{d}\Phi}{\mathrm{d}z} = -\dfrac{F^2}{2ES}$, where S is the cross-sectional surface area of the nanotube, whereas according to Clapeyron's theorem $F\mathrm{d}u = 2\mathrm{d}\Phi$. Thus, the following simple expression for the bundle composite strength ($\sigma_C = F_C/S$, effective stress and cross-sectional surface area are here considered; F_C is the force at fracture) is predicted:

$$\sigma_C^{(\text{theo})} = 2\sqrt{E\gamma\frac{P}{S}} \tag{18.14}$$

in which it appears as the ratio between the effective perimeter ($P = P_C + P_{vdW}$) in contact and the cross-sectional surface area of the nanotubes.

Equation (18.14) can be considered valid also for the entire bundle composite, since we are assuming here the same value P/S for all the nanotubes/graphene ribbons; the fact that the strength is not a function of the numbers or bundle composite size is for the same reason, i.e. because we are not assuming here a "defect" size distribution for S/P—that basically represents a characteristic defect size—but a constant value; of course, assuming a statistical distribution for the characteristic defect size S/P with the upper limit proportional to the structural size (the larger the structure the larger the largest defect) would imply a size effect, thus a dependence on the nanotube/graphene numbers or bundle composite size. Nevertheless, here we are interested in the simplest model (1) and in the upperbound strength predictions (2), thus we do not consider statistics into Eqn (18.14).

Note that Eqn (18.14) is basically the asymptotic elastic limit for sufficiently long overlapping length, that is, the length along with two adjacent nanotubes/graphene ribbons are nominally in contact; for overlapping length smaller than a critical value, the strength increases by increasing the overlapping length; for a single nanotube/graphene, this overlapping length is of the order of 10 μm, whereas it is expected to be larger for bundles/composites, (e.g. of the order of several millimeters, as confirmed experimentally). This critical length is $\ell_C \approx 6\sqrt{\dfrac{hES}{PG}}$ where h and G are the thickness and shear modulus of the interface, respectively. It suggests that increasing the size scale $L \propto \sqrt{S} \propto P \propto h$, this critical length increases too, namely $\ell \propto L$, thus the strength increases by increasing the overlapping length in a wider range; however, note that the achievable strength is reduced since, $\sigma_C^{(\text{theo})} \propto \sqrt{h}\ell^{-1} \propto \sqrt{P/S} \propto L^{-1/2}$, if $L \propto \ell \propto h$: increasing the overlapping length ad infinitum is not a way to indefinitely increase the strength. The real strength could be significantly smaller, not only because $\ell < \ell_C$ but also as a consequence of the misalignment of the nanotubes/graphene ribbons with respect to the bundle axis.

Assuming a nonperfect alignment in the bundle, described by a non-zero angle β (here assumed identical for all the nanotubes/graphene ribbons, even if—also in this case, as for the characteristic defect size S/P—a proper statistics could

be invoked for this parameter), the longitudinal force carried by the nanotubes/ graphene ribbons will be $F/\cos\beta$, thus the equivalent Young' modulus of the bundle/composite will be $E\cos^2\beta$, as can be evinced by the corresponding modification of the energy balance during delamination; accordingly,

$$\sigma_C = 2\cos\beta\sqrt{E\gamma\frac{P}{S}} \tag{18.15}$$

Applying eq. 18.15 to nanotubes, The maximal achievable strength is predicted for collapsed [45] perfectly aligned (sufficiently overlapped) nanotubes in a bundle or nanotubes even not collapsed in a composite, i.e. $\frac{P}{S} \approx \frac{1}{Nt}$, $\beta = 0$:

$$\sigma_C^{(\text{theo,N})} = 2\sqrt{\frac{E\gamma}{Nt}} \tag{18.16}$$

Taking $E = 1$ TPa (Young's modulus of graphene), $\gamma = 0.2$ N/m (surface energy of graphene; however, note that in reality, γ could be also larger as a consequence of additional dissipative mechanisms, e.g. fracture and friction in addition to adhesion, or presence of a matrix in a nanotube/graphene composites), the predicted maximum strength for single walled nanotube ($N = 1$) fiber/composite is $\sigma_C^{(\text{max,CNT})} = \sigma_C^{(\text{theo,1})} = 48.5$ GPa, whereas for double- or triple-walled nanotubes, $\sigma_C^{(\text{theo,2})} = 34.3$ GPa or $\sigma_C^{(\text{theo,3})} = 28.0$ GPa. For graphene, the surface area for load transfer is doubled with respect to the case of the single carbon nanotube (the inner surface area does not contribute) and thus from eqn (18.15) we predict [46],

$$\sigma_C^{(\text{max,G})} = \sqrt{2}\sigma_C^{(\text{max,CNT})} \tag{18.17}$$

This result is important and suggests that graphene is superior even to nanotubes for designing superstrong fibers and composites. These maximum stress predictions assume a vanishing matrix content in the fibers/composites; in general we expect:

$$\sigma_C^{(\text{Composite})} \cong \sigma_C^{(\text{G,CNT})}f + \sigma_C^{(\text{matrix})}(r - P)$$

where P is the volumetric content of graphene or carbon nanotubes in the composite.

18.11 **CONCLUSIONS**

The strength of a real, thus defective, carbon nanotube or graphene superstrong fibers is expected to be greatly reduced with respect to the theoretical strength of carbon nanotubes or graphene. Accordingly, in this chapter, key simple formulas for the design of superstrong carbon nanotube and graphene fibers and composites have been reviewed based on the analysis reported in previous papers by the same author. Graphene has been demonstrated to be superior even with respect to carbon nanotubes.

References

[1] Y.V. Artsutanov, Kosmos na elektrovoze, komsomol-skaya pravda. July 31 (1960); contents described in Lvov, V, Science 158 (1967) 946−947.

[2] J. Pearson, The orbital tower: a spacecraft launcher using the Earth's rotational energy, Acta Astronautica 2 (1975) 785−799.

[3] N. Pugno, On the strength of the nanotube-based space elevator cable: from nano-mechanics to megamechanics, Journal of Physics—Condensed Matter 18 (2006) S1971−S1990.

[4] N. Pugno, The role of defects in the design of the space elevator cable: from nanotube to megatube, Acta Materialia 55 (2007) 5269−5279.

[5] N. Pugno, Space elevator: out of order? Nano Today 2 (2007) 44−47.

[6] S. Iijima, Helical microtubules of graphitic carbon, Nature 354 (1991) 56−58.

[7] M.F. Yu, B.S. Files, S. Arepalli, R. Ruoff, Tensile loading of ropes of single wall carbon nanotubes and their mechanical properties, Physical Review Letters 84 (2000) 5552−5555.

[8] M.F. Yu, O. Lourie, M.J. Dyer, K. Moloni, T.F. Kelly, R. Ruoff., Strength and breaking mechanism of multiwalled carbon nanotubes under tensile load, Science 287 (2000) 637−640.

[9] B.C. Edwards, Design and deployment of a space elevator, Acta Astronautica 10 (2000) 735−744.

[10] B.C. Edwards, E.A. Westling, The Space Elevator: A Revolutionary Earth-to-Space Transportation System, Spageo Inc, 2003.

[11] N. Pugno, A Quantized Griffith's Criterion, Fracture Nanomechanics, Meeting of the Italian Group of Fracture, Vigevano, Italy, September 25−26, 2002.

[12] N. Pugno, R. Ruoff, Quantized fracture mechanics, Philosophical Magazine 84 (2004) 2829−2845.

[13] N. Pugno, Dynamic quantized fracture mechanics, International Journal of Fracture 140 (2006) 158−168.

[14] N. Pugno, New quantized failure criteria: application to nanotubes and nanowires, International Journal of Fracture 141 (2006) 311−328.

[15] N. Pugno, F. Bosia, A. Carpinteri, Multiscale stochastic simulations as in-silico tensile testing of nanotube-based megacables, Small 4 (2008) 1044-1052.

[16] N. Pugno, R. Ruoff, Nanoscale Weibull statistics, Journal of Applied Physics 99 (2006) 1−4.

[17] A. Carpinteri, Scaling laws and renormalization groups for strength and toughness of disordered materials, International Journal of Solid and Structures 31 (1994) 291−302.

[18] A. Carpinteri, N. Pugno, Are the scaling laws on strength of solids related to mechanics or to geometry? Nature Materials 4 (2005) 421−423.

[19] N. Pugno, A general shape/size-effect law for nanoindentation, Acta Materialia 55 (2007) 1947−1953.

[20] M. Ippolito, A. Mattoni, L. Colombo, N. Pugno, The role of lattice discreteness on brittle fracture: how to reconcile atomistic simulations to continuum mechanics, Physical Review B 73 (2006) 104111−1/6.

[21] D. Taylor, P. Cornetti, N. Pugno, The fracture mechanics of finite crack extensions, Engineering Fracture Mechanics 72 (2005) 1021−1028.

[22] N. Pugno, M. Ciavarella, P. Cornetti, A. Carpinteri, A unified law for fatigue crack growth, Journal of the Mechanics and Physics of Solids 54 (2006) 1333−1349.

[23] N. Pugno, P. Cornetti, A. Carpinteri, New unified laws in fatigue: from the Wöhler's to the Paris' regime, Engineering Fracture Mechanics 74 (2007) 595−601.

[24] J.R. Rice, G.F. Rosengren, Plane strain deformation near a crack tip in a power-law hardening material, Journal of the Mechanics and Physics of Solids 16 (1968) 1−12.

[25] A. Carpinteri, N. Pugno, Fracture instability and limit strength condition in structures with re-entrant corners, Engineering Fracture Mechanics 72 (2005) 1254−1267.

[26] A. Carpinteri, B. Chiaia, Crack-resistance behavior as a consequence of self-similar fracture topologies, International Journal of Fracture 76 (1996) 327−340.

[27] Q.Z. Wang, Simple formulae for the stress-concentration factor for two- and three-dimensional holes in finite domains, Journal of Strain Analysis 73 (2002) 259−264.

[28] N. Pugno, Young's modulus reduction of defective nanotubes, Applied Physics Letters 90 (2007) 043106.

[29] N. Pugno, H. Troger, A. Steindl, M. Schwarzbart, On the stability of the track of the space elevator, Proc. of the 57th International Astronautical Congress, October 2−6, 2007b, (Valencia, Spain).

[30] S.L. Mielke, D. Troya, S. Zhang, J.-L. Li, S. Xiao, R. Car, R.S. Ruoff, G.C. Schatz, T. Belytschko, The role of vacancy defects and holes in the fracture of carbon nanotubes, Chemical Physics Letters 390 (2004) 413−420.

[31] N. Pugno. Mimicking nacre with super-nanotubes for producing optimized super-composites. Nanotechnology 17 (2006) 5480-5484.

[32] T. Belytschko, S.P. Xiao, R. Ruoff, Effects of Defects on the Strength of Nanotubes: Experimental-Computational Comparisons, Los Alamos National Laboratory, 2002. Preprint Archive, Physics, arXiv:physics/0205090.

[33] S. Zhang, S.L. Mielke, R. Khare, D. Troya, R.S. Ruoff, G.C. Schatz, T. Belytschko, Mechanics of defects in carbon nanotubes: atomistic and multiscale simulations, Physical Review B 71 (2005) 115403 1−12.

[34] R. Khare, S.L. Mielke, J.T. Paci, S. Zhang, R. Ballarini, G.C. Schatz, T. Belytschko, Coupled quantum mechanical/molecular mechanical modelling of the fracture of defective carbon nanotubes and grapheme sheets, Physical Review B 75 (2007) 075412.

[35] W. Ding, L. Calabri, K.M. Kohlhaas, X. Chen, D.A. Dikin, R.S. Ruoff, Modulus, fracture strength, and brittle vs plastic response of the outer shell of arc-grown multiwalled carbon nanotubes, Experimental Mechanics 47 (2006) 25−36.

[36] M. Meo, M. Rossi, Tensile failure prediction of single wall carbon nanotube, Engineering Fracture Mechanics 73 (2006) 2589−2599.

[37] M. Sammalkorpi, A. Krasheninnikov, A. Kuronen, K. Nordlund, K. Kaski, Mechanical properties of carbon nanotubes with vacancies and related defects, Physical Review B 70 (2004) 245416−245421/8.

[38] W. Weibull, A statistical theory of the strength of materials, Ingeniörsvetens kapsakademiens, Handlingar 151 (1939).

[39] A.H. Barber, I. Kaplan-Ashiri, S.R. Cohen, R. Tenne, H.D. Wagner, Stochastic strength of nanotubes: an appraisal of available data, Composite Science and Technology 65 (2005) 2380−2386.

[40] I. Kaplan-Ashiri, S.R. Cohen, K. Gartsman, V. Ivanovskaya, T. Heine, G. Seifert, I. Wiesel, H.D. Wagner, R. Tenne, On the mechanical behavior of WS_2 nanotubes under axial tension and compression, Proceeding of the National Academy of Science USA 103 (2006) 523−528.

[41] C. Kittel, Introduction to Solid State Physics, John Wiley & Sons, New York, 1966.

[42] H.K.D.H. Bhadeshia, 52nd Hatfield memorial lecture—large chunks of very strong steel, Materials Science and Technology 21 (2005) 1293−1302.

[43] Y. Fan, B.R. Goldsmith, P.G. Collins, Identifying and counting point defects in carbon nanotubes, Nature Materials 4 (2005) 906−911.

[44] P.D. Beale, D.J. Srolovitz, Elastic fracture in random materials, Physical Review B 37 (1988) 5500−5507.

[45] N. Pugno, The design of self-collapsed super-strong nanotube bundles, Journal of the Mechanics and Physics of Solids 58 (2010) 1397−1410.

[46] N. Pugno, Towards the Artsutanov's dream of the space elevator: the ultimate design of a 35 GPa stronger tether thanks to graphene, Acta Astronautica (2012). (Available on line).